nature neuroscience

Regulation of chromatin accessibility and Zic binding at enhancers in the developing cerebellum

Christopher L Frank[1,2], Fang Liu[3], Ranjula Wijayatunge[3], Lingyun Song[2], Matthew T Biegler[3], Marty G Yang[3], Christopher M Vockley[2,4], Alexias Safi[2], Charles A Gersbach[2,5], Gregory E Crawford[2,6] & Anne E West[3]

To identify chromatin mechanisms of neuronal differentiation, we characterized chromatin accessibility and gene expression in cerebellar granule neurons (CGNs) of the developing mouse. We used DNase-seq to map accessibility of *cis*-regulatory elements and RNA-seq to profile transcript abundance across postnatal stages of neuronal differentiation *in vivo* and in culture. We observed thousands of chromatin accessibility changes as CGNs differentiated, and verified, using H3K27ac ChIP-seq, reporter gene assays and CRISPR-mediated activation, that many of these regions function as neuronal enhancers. Motif discovery in differentially accessible chromatin regions suggested a previously unknown role for the Zic family of transcription factors in CGN maturation. We confirmed the association of Zic with these elements by ChIP-seq and found, using knockdown, that Zic1 and Zic2 are required for coordinating mature neuronal gene expression patterns. Together, our data reveal chromatin dynamics at thousands of gene regulatory elements that facilitate the gene expression patterns necessary for neuronal differentiation and function.

Specialized cell function requires precise control of gene expression patterns. Chromatin regulation is involved in this process by establishing differential utilization of gene regulatory elements in cells of distinct fate lineages. Genome-wide studies have suggested that cell type–specific differences in gene expression are highly correlated with differences in both accessibility and activation state of distal gene enhancers[1,2]. These data have led to the hypothesis that developmental regulation of chromatin at enhancer elements mediates the process of cellular differentiation[3].

Neuronal differentiation is comprised of multiple steps, beginning with the commitment of neural stem cells to become specified neural progenitors, which then leave the cell cycle to become postmitotic neurons. Prenatal patterning of the brain is critically dependent on temporally and spatially restricted expression of transcription factors that act at brain region–selective enhancer elements[4,5]. By contrast, after birth, sensory experience-driven synaptic activity has an instructive role in initiating programs of gene expression that underlie neuronal maturation. This allows processes such as synapse development and excitatory/inhibitory balance in neural circuits to be adapted to the environment[6]. However, whether chromatin-dependent regulation of enhancer function contributes to gene expression that mediates these later stages of neuronal maturation remains largely unknown.

To fill this gap in knowledge, we used the differentiation of CGNs in the postnatal mouse cerebellum to identify chromatin-based transcriptional mechanisms that drive the maturation of neuronal gene expression programs. CGNs, which comprise >99% of cerebellar neurons, are derived during early postnatal life from committed granule neuron precursors (GNPs) that proliferate in the outer portion of the external granular layer of the developing cerebellar cortex[7]. Following exit from the cell cycle, GNPs differentiate into immature CGNs that migrate to the inner granular layer, where they form synaptic connections and then mature. These changes in CGN differentiation and function are accompanied by known changes in neuronal gene expression[8]. Notably, primary GNPs isolated from the postnatal mouse brain recapitulate discrete and synchronized stages of CGN differentiation in culture, providing a means for experimental validation and genetic manipulation of gene regulatory mechanisms that mediate this process[9,10].

DNase I hypersensitive (DHS) sites mark nucleosome-depleted regions that are universal hallmarks for gene regulatory elements, including promoters, enhancers, insulators and most transcription factor–binding sites[11]. We applied DNase-seq to globally map chromatin accessibility at key stages in the development of mouse cerebellum. We found that widespread changes in chromatin accessibility occurred as CGNs differentiated, marking dynamic enhancer elements that regulate the expression of genes necessary for proper neuronal function. In addition, we used our identification of these regions to determine a previously unknown role for the Zic transcription factors in coordinating the gene expression programs required for neuronal maturation.

[1]Department of Molecular Genetics and Microbiology, Duke University Medical Center, Durham, North Carolina, USA. [2]Center for Genomic and Computational Biology, Duke University Medical Center, Durham, North Carolina, USA. [3]Department of Neurobiology, Duke University Medical Center, Durham, North Carolina, USA. [4]Department of Cell Biology, Duke University Medical Center, Durham, North Carolina, USA. [5]Department of Biomedical Engineering, Duke University, Durham, North Carolina, USA. [6]Department of Pediatrics, Division of Molecular Genetics, Duke University Medical Center, Durham, North Carolina, USA. Correspondence should be addressed to G.E.C. (greg.crawford@duke.edu) or A.E.W. (west@neuro.duke.edu).

Received 26 January; accepted 12 March; published online 6 April 2015; doi:10.1038/nn.3995

RESULTS

Cerebellar development involves extensive chromatin remodeling

We used DNase-seq to globally map chromatin accessibility at three key stages in the development of the mouse cerebellum: postnatal day 7 (P7), when the external granular layer (EGL) of the mouse cerebellar cortex has reached its maximal thickness[12] as a result of the proliferation of GNPs (**Fig. 1a**); P14, when newborn postmitotic CGNs begin to populate the internal granule layer (IGL)[13]; and P60, when CGNs of the IGL express gene products that mediate mature synaptic functions[8] (**Fig. 1b**, **Supplementary Fig. 1a** and **Supplementary Table 1**). We identified approximately 70,000 DHS sites at each of the three developmental stages and found that these elements mapped to promoters, gene bodies and intergenic regions (**Supplementary Fig. 1b**). The majority of DHS sites (~77%) were found outside of annotated gene promoter regions, highlighting the ability of DNase-seq to identify distal regulatory elements in the genome.

To determine how chromatin accessibility changes during cerebellar differentiation, we assessed quantitative differences in DHS signal intensity between the three stages. We identified 24,886 total DHS sites that significantly 'opened' or 'closed' (gained or lost signal) during postnatal development (FDR < 0.05; **Fig. 1c,d**, **Supplementary Fig. 1c,d** and **Supplementary Table 2**). Similar to all DHS sites, developmentally regulated DHS sites were found in both proximal gene promoters and at intronic, exonic and intergenic regions (**Fig. 1e**). Notably, we found evidence of extensive chromatin remodeling between P14 and P60, even though these samples were primarily comprised of CGNs at two postmitotic stages of neuronal differentiation . These data indicate that there is extensive chromatin remodeling over the course of neuronal differentiation *in vivo* both as proliferating neural progenitors leave the cell cycle and as postmitotic neurons mature.

Although an advantage of cerebellar cortex is that it is predominantly composed of granule neurons (~85%), this brain region also contains astrocytes (~15%) and other kinds of neurons such as Purkinje cells (~0.2%)[7] (**Supplementary Fig. 2a,b**). To determine the effect of these other cell types on our chromatin analyses, we first

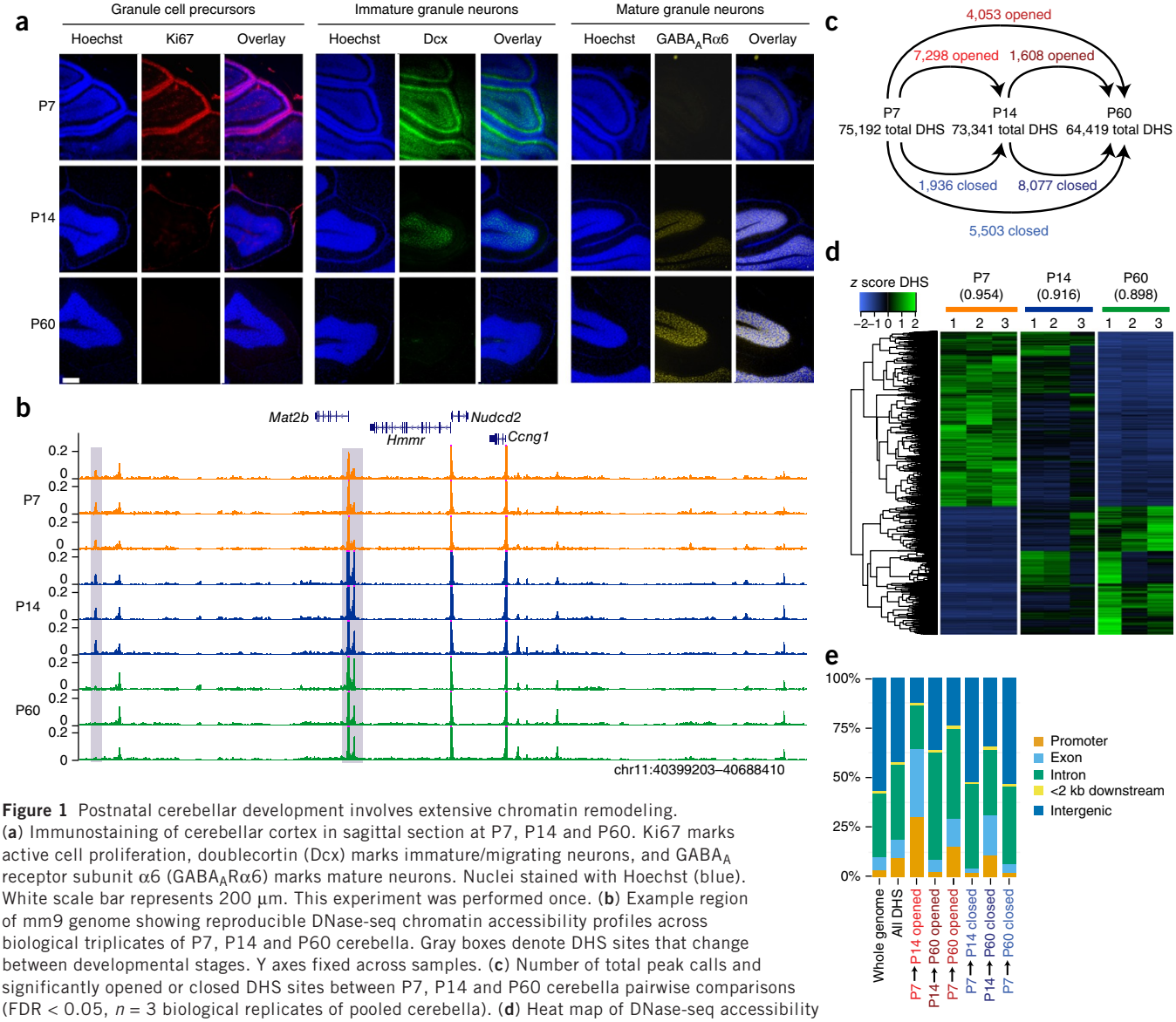

Figure 1 Postnatal cerebellar development involves extensive chromatin remodeling. (**a**) Immunostaining of cerebellar cortex in sagittal section at P7, P14 and P60. Ki67 marks active cell proliferation, doublecortin (Dcx) marks immature/migrating neurons, and GABA$_A$ receptor subunit α6 (GABA$_A$Rα6) marks mature neurons. Nuclei stained with Hoechst (blue). White scale bar represents 200 μm. This experiment was performed once. (**b**) Example region of mm9 genome showing reproducible DNase-seq chromatin accessibility profiles across biological triplicates of P7, P14 and P60 cerebella. Gray boxes denote DHS sites that change between developmental stages. Y axes fixed across samples. (**c**) Number of total peak calls and significantly opened or closed DHS sites between P7, P14 and P60 cerebella pairwise comparisons (FDR < 0.05, $n = 3$ biological replicates of pooled cerebella). (**d**) Heat map of DNase-seq accessibility across three time points for regions marked significant in DESeq analysis. Mean pairwise Pearson correlation between replicates listed above heat map. (**e**) Distribution of gene features for opened, closed and all identified DHS sites.

quantified aggregate DNase-seq signal at the promoters of genes that are preferentially expressed in CGNs, Purkinje neurons or Bergmann glia of the adult mouse cerebellum[14]. DNase signal was greatest at promoters of genes preferentially expressed in adult CGNs, suggesting that our DHS data represent chromatin state in this most abundant cell type (**Supplementary Fig. 2c**). Furthermore, when we considered the set of developmentally regulated DHS sites, these also had the strongest association with CGN-enriched genes (**Supplementary Fig. 2d**). ChIP-seq data sets obtained from mouse cerebellum were similarly enriched at CGN gene promoters over other cell types (**Supplementary Fig. 2e**,**f**).

As an additional way to control for cellular heterogeneity, we purified GNPs from the P7 cerebellum and differentiated these cells to CGNs in culture. These cultures are highly enriched for CGNs and depleted of glia and other kinds of neurons found in the cerebellar cortex *in vivo*[15]. Once plated, freshly dissociated GNPs rapidly exit the cell cycle[16] and synchronously differentiate, displaying characteristic neuronal morphologies by 3 d *in vitro* (+3 DIV) and forming synaptic connections by +7 DIV[17] (**Supplementary Fig. 3a**). We performed DNase-seq in triplicate on freshly isolated GNPs or GNPs that were cultured for 3 or 7 d and identified 28,119 differential DHS sites at FDR < 0.05 (**Supplementary Fig. 3b–d** and **Supplementary Table 3**). Similar to our findings from *in vivo* cerebellar samples, we found that opening and closing DHS sites in cultured CGNs are primarily non-promoter distal elements (**Supplementary Fig. 3e**). Although the majority (10,115 of 11,657 = 86.8%) of changes in DHS site accessibility occurred as GNPs left the cell cycle to become newborn CGNs, we also observed 1,542 (13.2%) DHS site changes that occurred between postmitotic +3 and +7 DIV samples. These data again indicate that postmitotic neurons can undergo substantial chromatin accessibility changes as they establish synapses and mature.

Comparing developmental regulation of DHS sites between the *in vivo* and culture systems revealed most sites exhibit matched direction of change (**Supplementary Fig. 4a**), but the magnitude of accessibility changes was generally lower in the cultured neurons. However, we also observed a cluster of DHS sites that closed gradually from P7 to P60 *in vivo*, but became transiently more accessible at +3 DIV before closing down at +7 DIV. Regulation of at least a subset of these sites accompanied transient increases in the expression of nearby genes. For example, *Grin2b* is a developmentally regulated NMDA-type glutamate receptor subunit that is most highly expressed in the neonatal brain, where it is important for the induction of long-term potentiation[18]. Two transiently opening DHS sites in an intron of the *Grin2b* gene parallel the transient increase in *Grin2b* mRNA expression at +3 DIV in cultured CGNs (**Supplementary Fig. 4b**,**c**). These data suggest that, in addition to reducing cellular heterogeneity, this culture system complements our *in vivo* differentiation analysis by improving temporal resolution of chromatin regulation during early steps in CGN differentiation.

Opening DHS sites mark mature CGN enhancers

To characterize the relationship between chromatin accessibility and regulation of gene expression in the developing cerebellum, we performed RNA-seq in triplicate from P7, P14 and P60 cerebellar cortex. Comparisons of gene expression levels between each stage confirmed robust transcriptional changes for 5,714 genes (FDR < 0.05) during postnatal cerebellar development (**Supplementary Fig. 5a**,**b** and

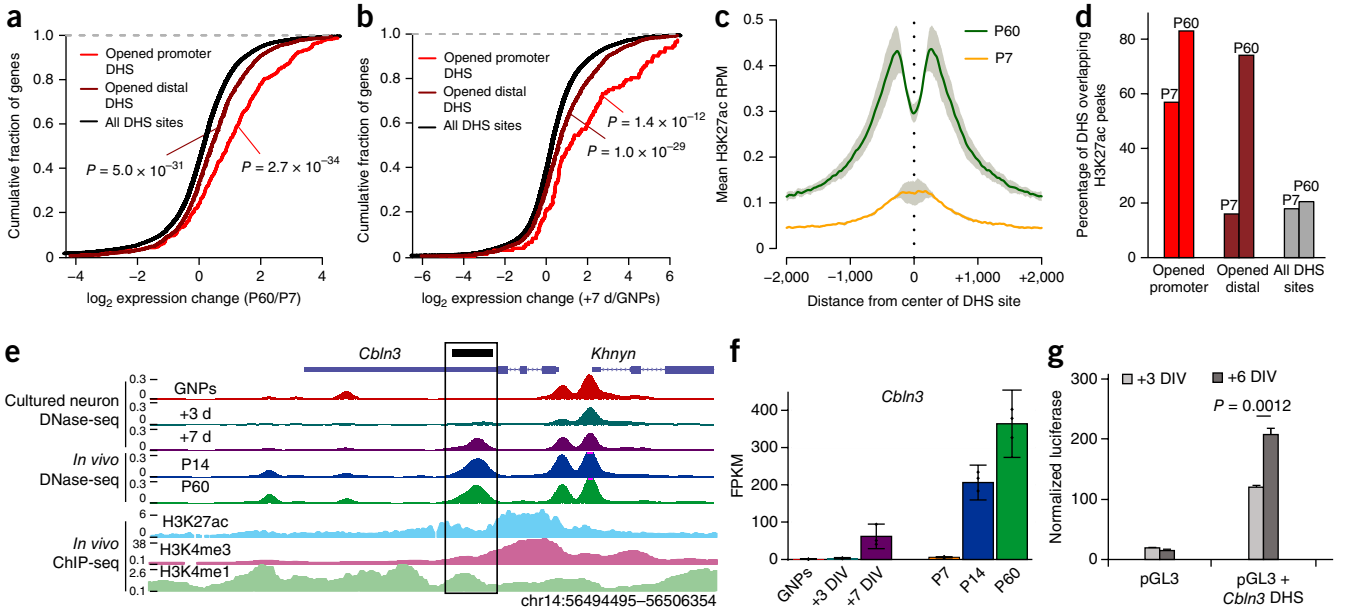

Figure 2 Opening DHS sites mark late-acting neuronal enhancers. (**a**,**b**) Cumulative fraction of genes nearest to opened promoter-located, opened distal and all identified DHS sites with given fold-change in RNA-seq expression from P7 to P60 cerebellum (**a**) or from GNPs to +7 DIV (**b**). Rightward shift indicates genes increased in expression across developmental time. Significance assessed by Mann-Whitney *U* test ($n = 3$ biological replicates of pooled cerebella). (**c**) Mean H3K27ac ChIP-seq signal (RPM, reads per million mapped) present at center of P7 to P60 opened DHS sites (4,053 sites) in either P7 cerebellum (orange line) or P60 cerebellum (green line). Gray = s.e.m. ($n = 2$ biological replicates of pooled cerebella). (**d**) Percent of opened promoter-located, opened distal and all DHS sites overlapping H3K27ac peaks identified in P7 or P60 cerebellum. (**e**) UCSC browser image highlighting a DHS site found in the 3′ UTR of *Cbln3* (black box), which opened during development and overlapped H3K27ac and H3K4me1 enrichment in adult cerebellum. (**f**) RNA-seq expression of *Cbln3* across developmental time *in vivo* and in cultured CGNs. Error bars represent 95% confidence interval. FPKM, fragments per kilobase of exon per million mapped. (**g**) Luciferase reporter assay for enhancer activity conferred by a DHS site in *Cbln3* at +3 DIV and +6 DIV. $P = 0.0012$ by two-sided Student's *t* test ($n = 3$ transfections, $t = 8.3$). Error bars represent s.e.m.

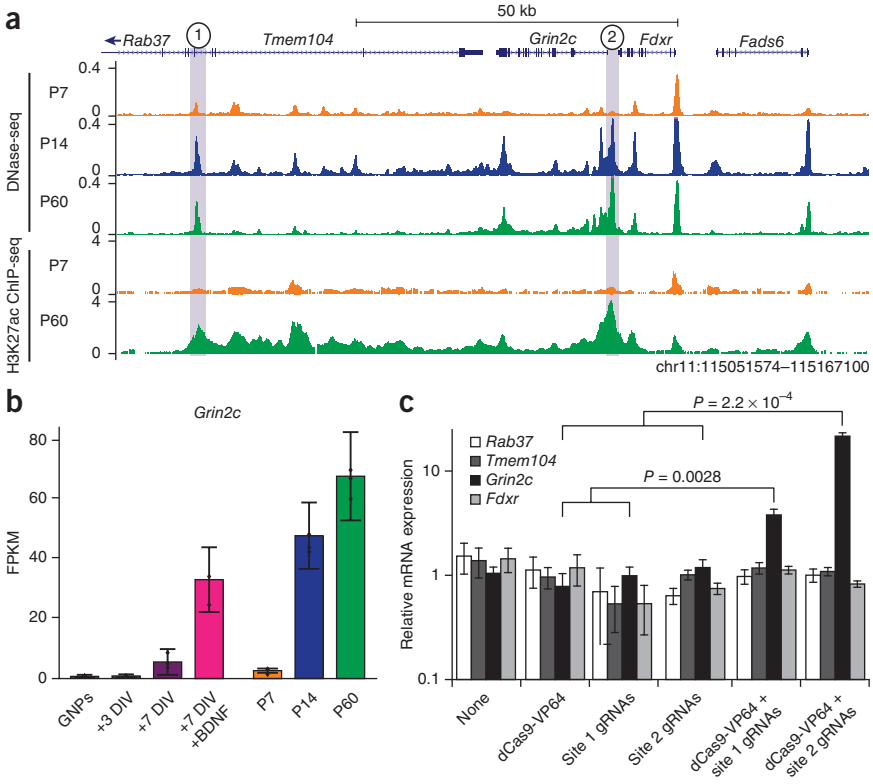

Figure 3 CRISPR-VP64–based activation confirms enhancer activity of late-opening DHS sites nearby *Grin2c*. (**a**) DNase-seq and H3K27ac ChIP-seq signal in vicinity of *Grin2c* with two DHS sites that opened across development and increased in H3K27ac signal marked in gray. (**b**) RNA-seq expression of *Grin2c* across developmental time *in vivo* and in culture. Error bars represent 95% confidence interval. (**c**) Cultured CGNs were either left uninfected (none) or were infected with dCas9-VP64 activator, three gRNAs targeting site #1 from (**a**), three gRNAs targeting site #2, or a combination of dCas9-VP64 and one of the two sets of gRNAs on +1 DIV, and harvested for qPCR on +7 DIV. All data were normalized to expression of *Gapdh* and scaled to average expression in control conditions (dCas9-VP64 or gRNAs only). $P = 0.0028$ for site 1 and $P = 0.00022$ for site 2 by two-sided Student's *t* test for dCas9-VP64 plus gRNAs versus dCas9-VP64 or gRNAs alone ($n = 5$ for dCas9-VP64 with gRNAs, $n = 8$ for site 1 controls, $n = 10$ for site 2 controls; $t = 5.5$ for site 1, $t = 12.3$ for site 2). Error bars represent s.e.m.

Supplementary Table 4). By clustering patterns of differentially expressed genes, we confirmed a number of previously described granule neuron gene expression dynamics and recovered gene ontologies descriptive of the differentiation process[19–22] (**Supplementary Fig. 5c–g** and **Supplementary Table 5**). As with our DNase-seq analysis, we also performed RNA-seq on triplicate replicates of purified GNPs that were either freshly isolated or differentiated in culture for +3 or +7 DIV. We found 1,972 differentially expressed genes in the cultures across this time course (**Supplementary Fig. 6a**), and principal components analysis of RNA-seq expression values placed +3 and +7 DIV samples in between GNPs and P14 cerebellum along an axis consistent with developmental time (**Supplementary Fig. 6b**).

We postulated that the developmentally regulated chromatin accessibility changes that we observed might mark a combination of promoter and enhancer elements that become activated at specific developmental stages to drive target gene expression. We first mapped each DHS site to its nearest gene and analyzed the relationship between that DHS site and the change in its associated gene expression value between P7 and P60. Although all DHS sites together exhibited a normal distribution of nearby gene expression changes centered on a fold change of 1, both promoter and distal DHS sites that opened up between P7 and P60 were significantly associated with genes that had higher expression levels at P60 ($P = 2.7 \times 10^{-34}$ and $P = 5.0 \times 10^{-31}$, respectively, Mann-Whitney test; **Fig. 2a**). Similar to our *in vivo* data, we found a strong association between GNP to +7 DIV opening DHS sites and increased nearby gene expression in cultured CGNs (**Fig. 2b**).

The functional identity of DHS sites (for example, enhancers, promoters and silencers) can be predicted by overlap with specific histone modifications[23,24]. With the knowledge that most DHS sites are located outside of proximal promoter regions, and that our opening

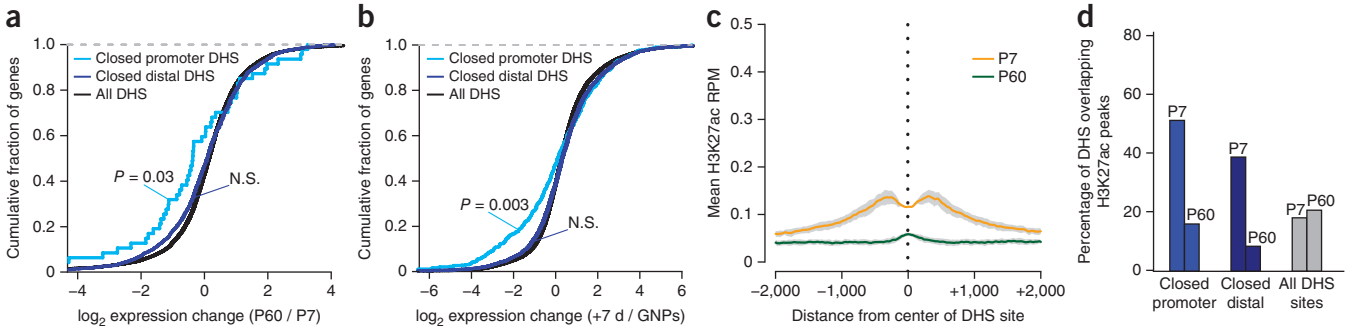

Figure 4 A subset of closing DHS sites mark early postnatal enhancer elements. (**a**,**b**) Cumulative fraction of genes nearest to closed promoter-located, closed distal and all identified DHS sites with given fold change in RNA-seq expression from P7 to P60 cerebellum (**a**) or from GNPs to +7 DIV (**b**). Leftward shift indicates genes decreased in expression across developmental time. Significance assessed by Mann-Whitney *U* test. N.S. indicates not significant, $P = 0.09$ and $P = 0.10$ for **a** and **b**, respectively. (**c**) Mean H3K27ac ChIP-seq signal (reads per million mapped) present at center of P7 to P60 closed DHS sites (5,503 sites) in either P7 cerebellum (orange line) or P60 cerebellum (green line). Gray = s.e.m. ($n = 2$ biological replicates of pooled cerebella). (**d**) Percent of closed promoter-located, closed distal and all DHS sites overlapping H3K27ac peaks identified in P7 or P60 cerebellum.

sites correlated with increased gene expression, we asked whether these sites colocalized with the enhancer mark H3K4me1 and the active enhancer/promoter modification H3K27ac. Comparing our developmentally regulated DHS sites to available mouse ENCODE ChIP-seq data from P56 cerebellum[25] revealed an enriched overlap between our opened DHS sites and the H3K4me1 (~77%, $P = 1.13 \times 10^{-120}$, hypergeometric test) and H3K27ac (~50%, $P = 8.82 \times 10^{-88}$) histone marks (**Supplementary Fig. 7a**). The combination of these two histone marks was particularly enriched in non-promoter opening DHS sites (~45% overlap peaks of both marks), whereas promoter-located opening DHS sites were enriched for H3K27ac in combination with H3K4me3 (~40% overlap peaks of both marks). This indicates that DHS sites that opened between P7 and P60 demarcate both active enhancers and promoters in adult cerebellum. To determine whether the opening of DHS sites over developmental time was associated with changing of histone marks, we performed ChIP-seq for H3K27ac in P7 and P60 cerebellum in duplicate. We found a strong correlation (Pearson's $r = 0.538$) between global H3K27ac and DHS signal changes in the developing cerebellum, indicating that increased accessibility is associated with concomitant H3K27ac deposition (**Supplementary Fig. 7b**,**c**). Separating out H3K27ac peaks that map to proximal promoters further revealed that the global correlation is driven primarily by non-promoter sites ($r = 0.278$ promoters versus $r = 0.621$ non-promoters; **Supplementary Fig. 7d**,**e**). Matching these observations, P7–P60-opened DHS sites contained a mean H3K27ac signal that increased markedly over development (**Fig. 2c**). Furthermore, the set of opening DHS sites was markedly enriched for overlap with H3K27ac peaks compared with all DHS sites at P60 (**Fig. 2d**). Together, these data suggest that increased chromatin accessibility is associated with the activation of enhancer elements that promote developmentally regulated increases in CGN gene expression.

To determine whether the opening DHS sites indeed function as enhancers of mature CGN gene expression, we first used luciferase assays to test the function of a DHS site that becomes significantly more accessible both *in vivo* and in culture found in the 3′ UTR of the cerebellin 3 precursor (*Cbln3*) gene, which encodes a secreted C1q-domain protein that modulates the formation, refinement and maintenance of CGN to Purkinje cell synapses[26,27] (**Fig. 2e**). This DHS site colocalized with the enhancer histone modifications H3K27ac and H3K4me1 in adult cerebellum and correlated with increased *Cbln3* expression over the course of CGN differentiation both in culture and *in vivo* (**Fig. 2e**,**f**). When cloned in front of a minimal promoter and transfected in CGNs, this element substantially increased luciferase expression (**Fig. 2g**). Furthermore, we found significantly more luciferase expression when we harvested neurons on +6 DIV compared with +3 DIV ($P = 0.0012$, Student's t test; **Fig. 2g**), indicating that the activity of this enhancer increases with the developmental maturation of the CGNs.

Next, to directly test the hypothesis that opening DHS sites represent enhancer elements in their native genomic context, we examined the locus surrounding the *Grin2c* gene on chromosome 11 in detail (**Fig. 3a**). In this interval, we identified two DHS sites that both opened and gained H3K27ac signal across postnatal development, one just upstream of the *Grin2c* promoter and the second in an intron of the nearby *Tmem104* gene. Of the four annotated genes in this region (*Tmem104*, *Grin2c*, *Fdxr* and *Fads6*), all were expressed in cerebellum, but only *Grin2c* expression was highly upregulated in differentiating CGNs, where it is a NMDA-type glutamate receptor subunit that mediates mature synaptic functions[19] (**Fig. 3b**, **Supplementary Table 6**). *Grin2c* expression can also be robustly induced by culturing CGNs for 7 d (+7 DIV) in the presence of brain-derived neurotrophic factor (BDNF), offering an opportunity to experimentally test transcriptional mechanisms of *Grin2c* regulation[28]. Notably, BDNF-induced gene expression changes occurred largely independent of changes in chromatin accessibility, as we observed only 33 opened and 6 closed DHS sites in response to BDNF exposure (**Supplementary Table 7**).

To determine whether the two identified DHS sites function as enhancers of *Grin2c* in their endogenous chromatin context, we used

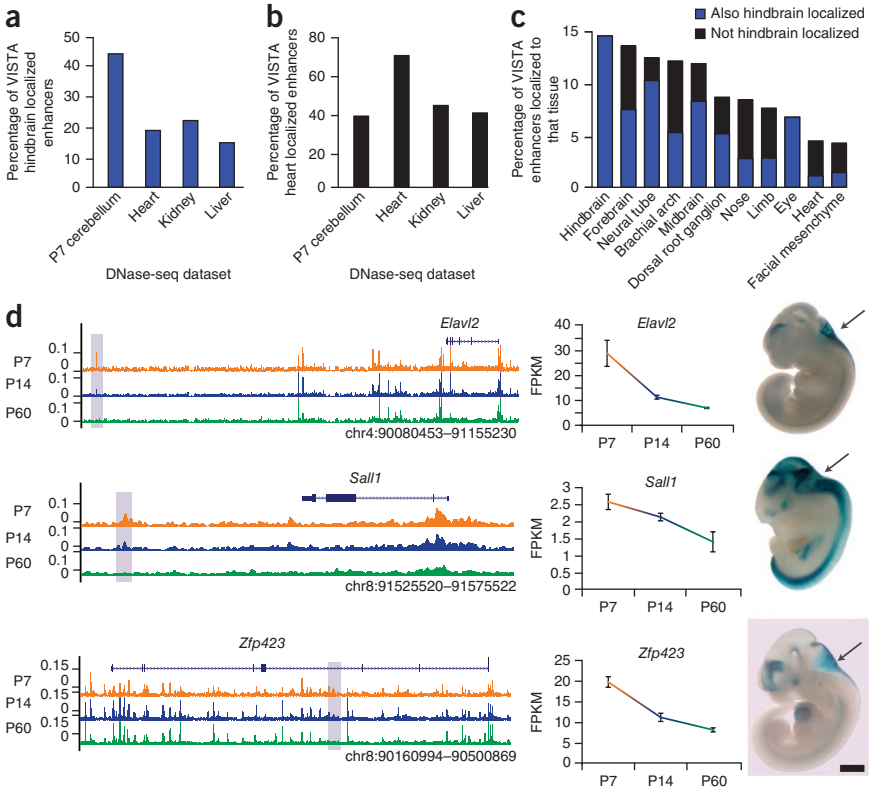

Figure 5 Postnatal closing DHS sites are enriched for embryonic hindbrain enhancer activity. (**a**,**b**) Percent of hindbrain (**a**) or heart (**b**) localized VISTA Enhancer Browser staining (embryonic day 11.5) covered by all DHS sites identified in P7 cerebellum, heart, kidney or liver mouse tissues (matching number of top peaks). (**c**) Percent of VISTA Enhancer Browser tissue-localized enhancers overlapped by DHS sites that close from P7 to P60. Tissues ordered by overlap rank. (**d**) Closed DHS sites located closest to the *Elavl2*, *Sall1* and *Zfp423* genes, all of which decrease in expression from P7 to P60 (center). Hindbrain expression is driven by each DHS site at E11.5, as seen with LacZ (blue) staining of embryos on right. Black scale bar represents 1 mm. Images sourced from VISTA Enhancer Browser: hs643, hs152 and hs625. Error bars represent s.e.m.

a CRISPR RNA-guided method to recruit a synthetic dCas9-linked transcriptional activator to each of the two putative enhancers flanking *Grin2c* in cultured CGNs[29]. Co-infection of dCas9-VP64 with CRISPR guide RNAs (gRNAs) targeting either site was sufficient to induce a selective upregulation of *Grin2c* expression compared with levels in control-infected neurons (**Fig. 3c**). By contrast, expression of three other nearby genes (*Rab37*, *Tmem104* and *Fdxr*) remained unchanged. Together, our CRISPR data indicate that two developmentally regulated DHS sites, including one located >50 kb away from the *Grin2c* promoter, act as gene-specific enhancers, highlighting the power of our comparative DHS analysis to locate physiologically relevant enhancers of important neuronal genes.

Early-acting enhancers are deactivated before closing

In contrast with the opening DHS sites, we observed only a modest association between DHS sites that close between P7 and P60 and the expression of their nearest gene ($P = 0.03$ promoter located, $P = 0.09$ for distal) or from GNPs to +7 DIV ($P = 0.003$ promoter-located, $P = 0.10$ for distal) (**Fig. 4a**,**b**). As expected, closing DHS sites largely did not colocalize with the enhancer markers H3K4me1 and H3K27ac in P56 brain (**Supplementary Fig. 7a**). However, these regions did exhibit somewhat greater H3K27ac ChIP-seq signal in P7 cerebellum than at P60, with decreases in this active enhancer mark being noted over the course of development at both promoter-located and distal DHS sites (**Fig. 4c**,**d**). These data suggest that at least a subset of the closing DHS sites are likely to be active enhancers in GNPs that are deactivated as CGNs differentiate. However, given that we observed noticeably less H3K27ac enrichment at P7 for closing DHS sites compared with the enrichment of H3K27ac at P60 for opening DHS sites, we considered the possibility that the loss of chromatin accessibility may slowly follow the functional deactivation of enhancer elements.

If this is the case, then the closing DHS sites may mark regions that function as enhancers in earlier stages in hindbrain development before the differentiation of GNPs. To test this hypothesis, we queried the VISTA Enhancer Browser, which contains enhancer elements that have been validated for their ability to drive tissue-restricted *in vivo* expression at embryonic day 11.5 (E11.5)[30]. At this age, the proliferative neuroepithelial cells of the cerebellar primordium are found at the rostral end of the rhomencephalon surrounding the fourth ventricle[7]. We therefore looked for overlap between our closing DHS sites and VISTA enhancers validated for their transcriptional activity in this region of the E11.5 embryo. We found that VISTA hindbrain-expressing enhancers overlapped more with P7 cerebellum DHS sites (108 of 242, 44.6%) compared with DHS sites from mouse heart (19%), kidney (22.3%) or liver (14.9%) (**Fig. 5a**). In contrast, VISTA heart enhancers overlapped more with mouse heart DHS sites than DHS sites from P7 cerebellum, kidney or liver (**Fig. 5b**). Notably, DHS sites that close in cerebellum between P7 and P60 displayed the highest overlap with enhancers that function in hindbrain (14.9%), forebrain (13.8%) and neural tube (12.7%) at E11.5, and a lower overlap with enhancers that function in non-neuronal tissues (**Fig. 5c**). This is in marked contrast with DHS sites that opened between P7 and P60, which overlapped only 1.7% of the E11.5 hindbrain enhancers (**Supplementary Table 8**).

Of the 36 DHS sites that both closed during postnatal cerebellar development and drove hindbrain expression at E11.5, we found 13 (36%) nearest to a gene that displayed significantly decreased expression from P7 to P60 (FDR < 0.05; **Fig. 5d** and **Supplementary Table 8**). This list of associated genes included *Elavl2* (HuB), which encodes an RNA-binding protein involved in neuronal development[31], *Sall1*, which encodes a zinc-finger transcription factor, mutations in which are associated with developmental disorders and cognitive deficits in humans[32], and *Zfp423*, which encodes a zinc-finger protein that is required for normal cerebellar development[33]. These data provide important experimental support for our hypothesis that many of the DHS sites that close during postnatal cerebellar development serve as enhancers of genes that function early in hindbrain development and further suggests that functional deactivation of these enhancers precedes DHS site closure.

Zics bind developmentally regulated DHS sites

Developmental regulation of chromatin architecture is thought to determine gene regulatory element accessibility to transcription

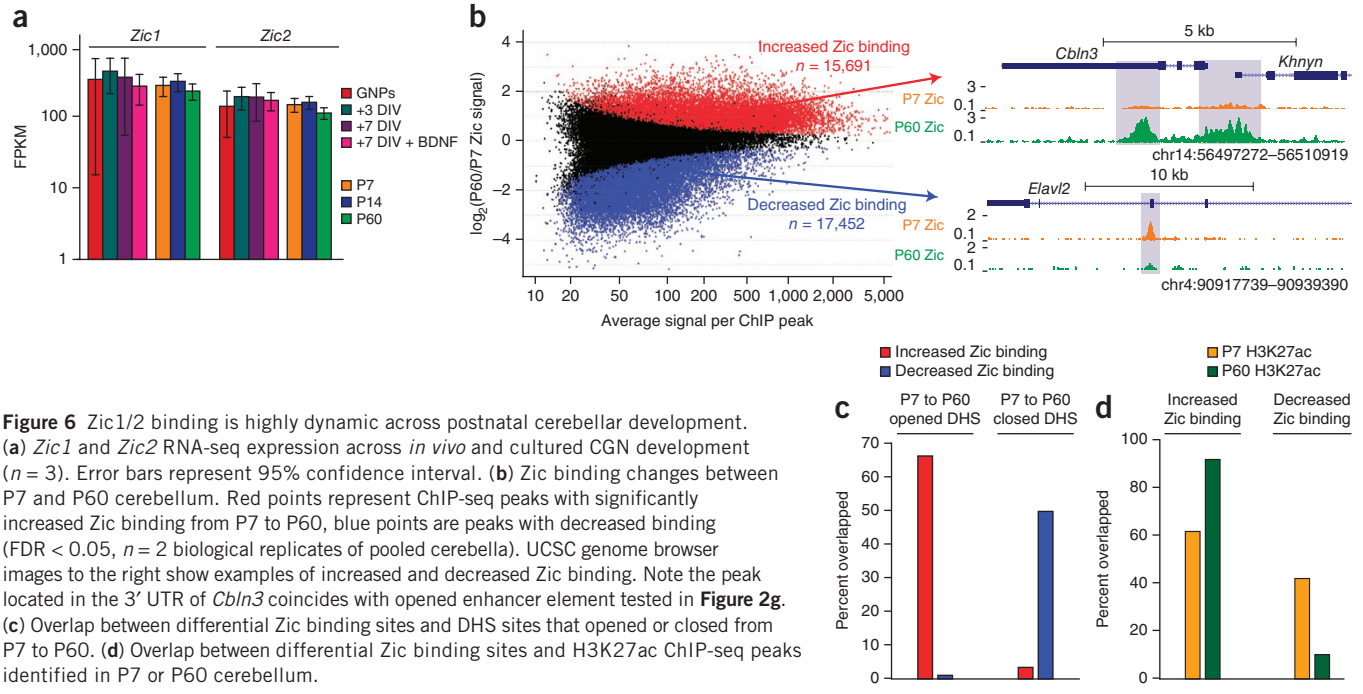

Figure 6 Zic1/2 binding is highly dynamic across postnatal cerebellar development. (**a**) *Zic1* and *Zic2* RNA-seq expression across *in vivo* and cultured CGN development ($n = 3$). Error bars represent 95% confidence interval. (**b**) Zic binding changes between P7 and P60 cerebellum. Red points represent ChIP-seq peaks with significantly increased Zic binding from P7 to P60, blue points are peaks with decreased binding (FDR < 0.05, $n = 2$ biological replicates of pooled cerebella). UCSC genome browser images to the right show examples of increased and decreased Zic binding. Note the peak located in the 3′ UTR of *Cbln3* coincides with opened enhancer element tested in **Figure 2g**. (**c**) Overlap between differential Zic binding sites and DHS sites that opened or closed from P7 to P60. (**d**) Overlap between differential Zic binding sites and H3K27ac ChIP-seq peaks identified in P7 or P60 cerebellum.

factor binding[1,34,35]. We therefore sought to identify transcription factors whose regulatory functions may be dictated by chromatin accessibility changes by searching for enrichment of transcription factor motifs in DHS sites that opened or closed between P7 and P60 *in vivo*, as well as those that opened or closed over 7 d of GNP differentiation in culture.

As expected, motifs for the MEF2 and NF1 families, which have been shown to be important for CGN differentiation[9,36], were enriched in both opening and closing DHS sites (**Supplementary Fig. 8**). However, we were surprised to find the zinc finger in cerebellum (Zic) transcription factor family motifs enriched in the set of opening DHS sites. Mutations in the human *ZIC* genes have been associated with cerebellar development disorders, suggesting their importance in CGN differentiation, and mouse knockout studies have indicated that the Zics function in GNPs to prevent their premature exit from the cell cycle[37,38]. However, the Zic transcription factors remain highly expressed in differentiated CGNs (**Fig. 6a**), raising the possibility that these factors also contribute to later stages in CGN maturation. Given our observation that the Zic motif was enriched in opening DHS sites, we hypothesized that the Zic transcription factors might change their gene targets over time by binding to developmentally regulated DHS sites.

To determine whether Zic transcription factors are differentially bound to DHS sites as CGNs differentiate, we performed ChIP-Seq from P7 or P60 cerebellum using an antibody specific for Zic1 and Zic2 (ref. 39) (**Supplementary Fig. 9a**,**b**). As a control, no significant peaks were observed with IgG pulldown from P7 or P60 cerebellum or when we performed Zic ChIP-seq from P60 cortex, where Zic1 and Zic2 are not expressed (**Supplementary Fig. 9c**). Although 60% of ChIP-seq peaks overlapped between P7 and P60 (**Supplementary Fig. 10a**,**b**), we found over 15,000 peaks with significantly (FDR < 0.05) increased or decreased ChIP signal at P60 compared with P7 cerebellum (**Fig. 6b** and **Supplementary Table 9**). These data demonstrate that Zic transcription factors undergo dynamic changes in their DNA binding patterns in the developing cerebellum despite constant levels of expression.

Consistent with the enrichment of Zic-binding motifs in opening DHS sites, we found that ~65% (2,683 of 4,053) of the opening DHS sites overlapped with Zic peaks that displayed stronger ChIP signal at P60. By contrast, less than 1% (36 of 4,053) of the opening DHS sites overlapped with Zic peaks with decreased ChIP signal across this time period (**Fig. 6c**). We also found nearly 50% (2,735 of 5,503) of closing DHS sites showed decreases in Zic binding, whereas only ~3% (179 of 5,503) showed stronger Zic association over time. Increases and decreases in Zic binding over developmental time were correlated with H3K27ac signal, suggesting that Zic contributes to the enhancer activity of these elements (**Fig. 6d**). Taken together, these data suggest that the chromatin-regulated binding of Zic transcription factors to enhancers may contribute to differential regulation of gene transcription during CGN differentiation.

Zics promote mature neuronal transcription

To test whether Zic is required for regulation of gene expression during CGN development, we returned to examining the ~120-kb region surrounding the *Grin2c* gene, where we observed strong Zic ChIP-seq peaks in P60 cerebellum directly overlapping the two sites tested for enhancer function (**Fig. 7a**). To determine whether Zic is required for the developmental upregulation of *Grin2c* expression, we used lentiviral shRNAs to knockdown Zic1 and/or Zic2 expression in cultured CGNs (**Supplementary Fig. 9a**,**b**). Knockdown of either Zic1 or Zic2, or both together significantly reduced the expression of *Grin2c* compared with control-infected neurons (**Fig. 7b**). To test the role of Zic in the two DHS sites that we found to be *Grin2c* enhancers specifically, we cloned each element into a minimal promoter luciferase reporter plasmid, transfected them into cultured CGNs, and measured luciferase activity 3 or 6 d later. Both elements demonstrated enhancer activity at +6 DIV (**Fig. 7c**) and knockdown of Zic1 significantly reduced the enhancer activity of both sites ($P = 0.0026$ and $P = 0.0042$, Student's t test; **Fig. 7c**). Thus, the developmentally regulated recruitment of Zic to these regions is functionally important for these elements to induce transcription.

Finally, given the high degree of overlap between opening DHS sites and increased Zic1 and Zic2 binding as CGNs mature (**Fig. 6c**), we hypothesized that Zic might function to globally coordinate the maturation of gene expression programs in differentiating CGNs. Consistent with this hypothesis, we found a significant association between increased Zic binding and developmental upregulation of nearby gene expression (**Fig. 8a**). The relationship between Zic binding and gene expression was strongest when multiple differential Zic binding sites mapped to a single gene (**Fig. 8b**). To determine the requirement for Zic in CGN differentiation, we used RNA-seq to analyze the effects of Zic1 or Zic2 knockdown on global gene expression in cultured CGNs. Knockdown of either Zic1 or Zic2 drove significant changes in the expression of 81 and 147 genes, respectively (FDR < 0.10;

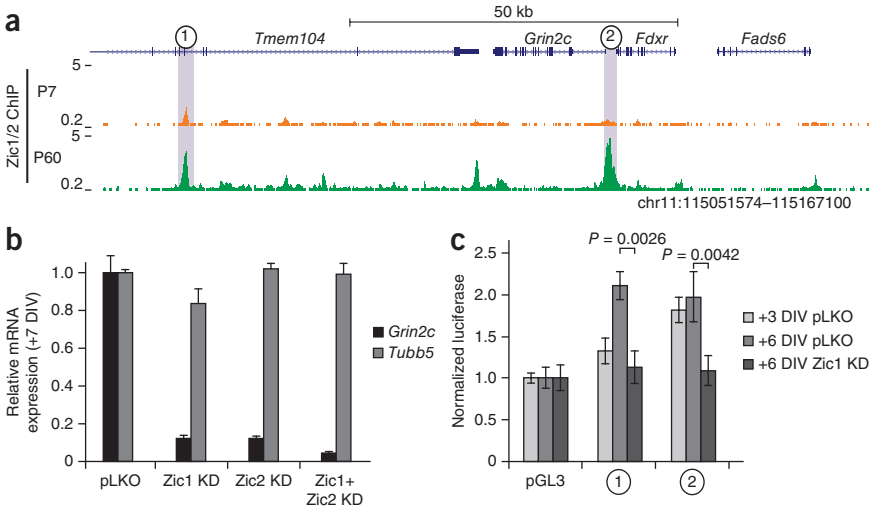

Figure 7 *Grin2c* transcription is controlled by Zic1/2 stage-specific access to enhancer elements. (**a**) Zic1/2 ChIP-seq signal in the vicinity of *Grin2c*. The two sites highlighted in gray increased in accessibility, gained H3K27ac and increased in Zic1/2 affinity during development from P7 to P60 cerebellum (also see **Fig. 3a**). (**b**) qRT-PCR *Grin2c* expression levels in culture at +7 DIV following Zic1, Zic2 or combined Zic1 and Zic2 knockdown (KD) by shRNA, compared with empty vector (*pLKO*). *Tubb5* used as control for total neuron number. Error bars represent s.e.m. ($n = 3$ cultures). (**c**) Luciferase reporter assay for DHS sites highlighted in **a** in cultured neurons. Both sites were sufficient to confer enhancer activity that was reduced by Zic1 knockdown at +6 DIV. Error bars represent s.e.m. $P = 0.0026$ for site 1 and $P = 0.0042$ for site 2 by two-sided Student's t test for Zic1 KD versus *pLKO* control ($n = 3$ transfections, $t = 6.7$ and 5.8).

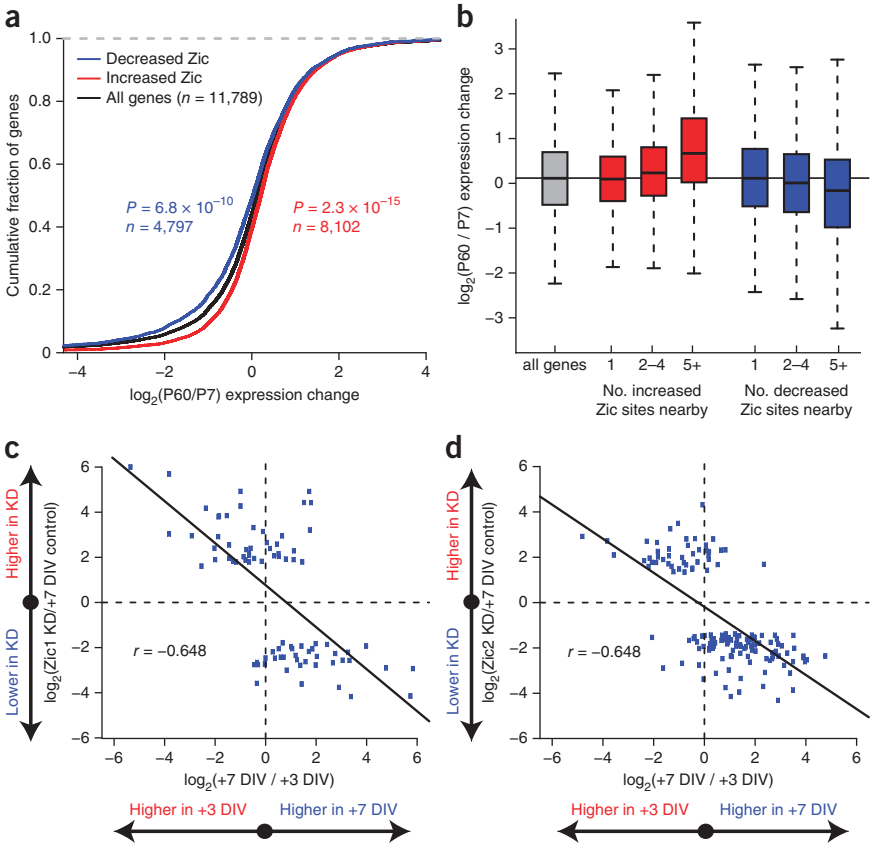

Figure 8 Zic1/2 promote the mature CGN transcriptional program. (**a**) Relationship between Zic binding changes and nearby gene RNA-seq expression changes from P7 to P60. Significance of shifts was assessed by two-sided Mann-Whitney *U* test. (**b**) Boxplots of gene expression change from P7 to P60 cerebellum were binned by number of Zic binding sites associated with each gene. Having multiple Zic binding changes nearby was more strongly associated with directional gene expression changes than single sites. Center line represents the median, box limits represent the first and third quartiles, and whiskers represent 1.5 times the interquartile range. (**c**,**d**) Relationship between cultured CGN development and *Zic1* (**c**) or *Zic2* (**d**) shRNA knockdown for genes marked significant in knockdown RNA-seq experiments (FDR < 0.10, $n = 2$ independent cultures). X axis shows fold change in gene expression between +3 DIV and +7 DIV in cultured CGNs. Y axis shows fold change in gene expression between control infected and Zic1 or Zic2 knockdown. Both knockdowns exhibited negative Pearson correlation coefficients (*r*).

Supplementary Table 10). To determine how this set of Zic-regulated genes was related to the gene expression changes that accompany CGN differentiation, we plotted the expression change of each Zic-regulated gene between +3 DIV and +7 DIV in control cultures versus the expression change for that same gene at +7 DIV after knockdown of Zic1 (**Fig. 8c**) or Zic2 (**Fig. 8d**). These data reveal that genes that show reduced expression following Zic1 or Zic2 knockdown tended to be upregulated over the time course of CGN differentiation, whereas genes with higher expression following Zic1 or Zic2 knockdown tended to be downregulated over the course of differentiation. Thus, the net effect of Zic1 or Zic2 knockdown is a shift in the gene expression program toward a less mature pattern. Overall, these data indicate that Zic recruitment to regions of opened chromatin is essential for the maturation of gene expression programs in differentiating CGNs.

DISCUSSION

Mammalian genomes harbor over a million *cis*-regulatory elements in total[11]. Previous studies comparing hundreds of diverse cell and tissue types demonstrate that the selective accessibility of these sites dictates cell-type identity and function[1,34,35]. Developmentally regulated mammalian chromatin accessibility changes have previously been studied in the context of purified cell lineages like intestinal epithelium[40] and $CD4^+$ T cells[41]. Here we focused our analysis on a single neuronal cell lineage to map the *in vivo* chromatin accessibility changes that occur during development. Our data reveal that chromatin accessibility is highly dynamic across both early and postmitotic stages of neuronal maturation. We found accessibility to be strongly linked to H3K4me1 and H3K27ac deposition outside of promoters, indicating that these chromatin accessibility changes identify regions that are enriched for poised and active enhancer elements. We demonstrated the value of identifying these dynamic DHS sites by predicting and validating a previously unknown role for the Zic transcription factors in neuronal maturation, thus enriching our mechanistic understanding of brain development. The identification of postmitotic neuronal changes in enhancer accessibility and regulation raises the possibility that this form of chromatin plasticity could contribute to transcription-dependent forms of learning and memory in the adult brain.

We found that, although DHS site opening frequently coincided with an increase both in H3K27ac signal and transcription of nearby genes, DHS site closing correlated weakly with decreasing gene expression and predominantly occurred at elements that already lacked H3K27ac at P7. At least a subset of these closing elements functioned as enhancers in the cerebellar primordium during embryonic stages of brain development, suggesting that enhancer deactivation precedes the loss of accessibility. This evidence that an epigenetic signature is retained in the form of chromatin accessibility at some enhancers, even though they are no longer active, could permit the reactivation of gene expression programs otherwise thought to be cell type or developmental stage specific.

We observed a substantial difference in the magnitude to which DHS sites opened in CGNs that were differentiated in culture compared with *in vivo*. This suggests that full maturation of CGN chromatin accessibility requires cell non-autonomous factors in the developing cerebellum. These external influences could include interactions with the Purkinje neurons, which are important for the proliferation and migration of CGNs, as well as patterned neural activity arising from sensory input to the intact brain, which have a key role in refining cerebellar synapses[42]. Further elucidating the role of extrinsic factors in the regulation of chromatin accessibility is likely to uncover mechanisms of gene-environment interactions relevant to both normal and abnormal brain development.

Differential DHS analysis allowed us to predict and confirm that members of the Zic transcription factor family preferentially bind DHS sites that open during CGN differentiation. Mice lacking Zic1 alone or in combination with Zic2 have a small cerebellum, indicating a requirement for the Zics in the normal proliferation of cerebellar GNPs[43].

Heterozygous loss-of-function mutations in *ZIC1* and *ZIC4* have been identified in patients with Dandy-Walker malformation, a congenital malformation of the cerebellum[37], further demonstrating fundamental roles for these transcription factors in brain development. However, our evidence that Zics act in postmitotic CGNs to promote mature gene expression patterns was surprising in light of previous studies that have demonstrated a role for the Zics in preventing premature differentiation of dividing neuronal precursors[43,44].

Zic family member expression remained constant throughout CGN development, yet these factors had distinct genome binding profiles at P7 and P60. Our evidence that sites of regulated Zic binding overlapped developmentally regulated DHS sites suggests that chromatin accessibility determines local Zic affinity. Developmental changes in chromatin accessibility are thought to be mediated by pioneer transcription factors that first recognize their sequence-specific DNA binding sites and then recruit chromatin-remodeling complexes[45]. Our data show that many gene regulatory elements that recruit Zic binding between P7 and P60 already overlapped the active enhancer mark H3K27ac at P7, although they further increase in H3K27ac signal over development. These data raise the possibility that other developmentally regulated factors bind these sites first, and then recruit Zic. The switch in Zic binding sites may explain how Zics get repurposed for two very different functions—inhibition of premature differentiation in GNPs and promotion of maturation in post-mitotic CGNs—at distinct steps in the differentiation of the same cell lineage. Although the Zics are widely expressed in the developing brain, CGNs are one of the few kinds of neurons that maintain Zic expression in adulthood, suggesting that other transcription factors may function at stage-specific enhancers to direct mature neuronal gene expression programs in other types of neurons.

Although previous studies have demonstrated that extracellular signal–regulated transcription factors can drive CGN maturation[9,36,46,47], the contributions of chromatin accessibility dynamics to these processes have not been investigated. The idea that environmental stimuli can induce changes in chromatin accessibility has been called into question by studies that have shown that stimulus-dependent changes in gene transcription, for example, those induced by glucocorticoid hormones[48] or exposure of intestinal epithelia to microbiota[49], can occur independent of changes in chromatin accessibility. However, we found that DHS sites changed substantially during the late stages of postmitotic CGN maturation. Given that these late stages of differentiation are primarily driven by the action of stimulus-regulated transcription factors[9,36,46,47], this implies that at least a subset of environmental stimuli are capable of driving changes in chromatin accessibility. The identification of these environmental factors and how they interact with Zic and other transcription factors will be important for understanding neuronal development, plasticity and disease.

METHODS

Methods and any associated references are available in the online version of the paper.

Accession codes. Sequencing data have been deposited at Gene Expression Omnibus (GEO) under accession number GSE60731.

Note: Any Supplementary Information and Source Data files are available in the online version of the paper.

ACKNOWLEDGMENTS

We thank the Duke Genome Sequencing and Analysis Core for sequencing the RNA-seq, ChIP-seq and DNase-seq libraries. This work was supported by the Duke Institute for Brain Sciences, and US National Institutes of Health grants 1R21NS084336 (A.E.W. and G.E.C.) and R01DA036865 (C.A.G. and G.E.C).

AUTHOR CONTRIBUTIONS

A.E.W., G.E.C., C.L.F., R.W. and F.L. designed the study. F.L., C.L.F., R.W., L.S. and A.S. performed DNase-seq and ChIP-seq experiments. M.T.B., M.G.Y., C.M.V. and C.A.G. designed and performed targeted enhancer function assays. F.L. performed Zic knockdown experiments. C.L.F. performed all bioinformatic analyses. C.L.F., A.E.W. and G.E.C. wrote the manuscript with input from all authors.

COMPETING FINANCIAL INTERESTS

The authors declare no competing financial interests.

1. Song, L. *et al.* Open chromatin defined by DNaseI and FAIRE identifies regulatory elements that shape cell-type identity. *Genome Res.* **21**, 1757–1767 (2011).
2. Heintzman, N.D. *et al.* Histone modifications at human enhancers reflect global cell type–specific gene expression. *Nature* **459**, 108–112 (2009).
3. Levine, M., Cattoglio, C. & Tjian, R. Looping back to leap forward: transcription enters a new era. *Cell* **157**, 13–25 (2014).
4. Gray, P.A. *et al.* Mouse brain organization revealed through direct genome-scale TF expression analysis. *Science* **306**, 2255–2257 (2004).
5. Pattabiraman, K. *et al.* Transcriptional regulation of enhancers active in protodomains of the developing cerebral cortex. *Neuron* **82**, 989–1003 (2014).
6. West, A.E. & Greenberg, M.E. Neuronal activity-regulated gene transcription in synapse development and cognitive function. *Cold Spring Harb. Perspect. Biol.* **3**, a005744 (2011).
7. Altman, J. & Bayer, S.A. *Development of the Cerebellar System: In Relation to its Evolution, Structure, and Functions* (CRC Press, 1997).
8. Hatten, M.E. & Heintz, N. Mechanisms of neural patterning and specification in the developing cerebellum. *Annu. Rev. Neurosci.* **18**, 385–408 (1995).
9. Ding, B. *et al.* Temporal regulation of nuclear factor one occupancy by calcineurin/NFAT governs a voltage-sensitive developmental switch in late maturing neurons. *J. Neurosci.* **33**, 2860–2872 (2013).
10. Kuhar, S.G. *et al.* Changing patterns of gene expression define four stages of cerebellar granule neuron differentiation. *Development* **117**, 97–104 (1993).
11. Thurman, R.E. *et al.* The accessible chromatin landscape of the human genome. *Nature* **489**, 75–82 (2012).
12. Altman, J. Autoradiographic and histological studies of postnatal neurogenesis. 3. Dating the time of production and onset of differentiation of cerebellar microneurons in rats. *J. Comp. Neurol.* **136**, 269–293 (1969).
13. Gleeson, J.G., Lin, P.T., Flanagan, L.A. & Walsh, C.A. Doublecortin is a microtubule-associated protein and is expressed widely by migrating neurons. *Neuron* **23**, 257–271 (1999).
14. Mellén, M., Ayata, P., Dewell, S., Kriaucionis, S. & Heintz, N. MeCP2 binds to 5hmC enriched within active genes and accessible chromatin in the nervous system. *Cell* **151**, 1417–1430 (2012).
15. Hatten, M.E. Neuronal regulation of astroglial morphology and proliferation *in vitro*. *J. Cell Biol.* **100**, 384–396 (1985).
16. Fogarty, M.P., Emmenegger, B.A., Grasfeder, L.L., Oliver, T.G. & Wechsler-Reya, R.J. Fibroblast growth factor blocks Sonic hedgehog signaling in neuronal precursors and tumor cells. *Proc. Natl. Acad. Sci. USA* **104**, 2973–2978 (2007).
17. Fletcher, T.L., De Camilli, P. & Banker, G. Synaptogenesis in hippocampal cultures: evidence indicating that axons and dendrites become competent to form synapses at different stages of neuronal development. *J. Neurosci.* **14**, 6695–6706 (1994).
18. Yashiro, K. & Philpot, B.D. Regulation of NMDA receptor subunit expression and its implications for LTD, LTP and metaplasticity. *Neuropharmacology* **55**, 1081–1094 (2008).
19. Farrant, M., Feldmeyer, D., Takahashi, T. & Cull-Candy, S.G. NMDA-receptor channel diversity in the developing cerebellum. *Nature* **368**, 335–339 (1994).
20. Ruppert, C., Goldowitz, D. & Wille, W. Proto-oncogene c-myc is expressed in cerebellar neurons at different developmental stages. *EMBO J.* **5**, 1897–1901 (1986).
21. Eroglu, C. *et al.* Gabapentin receptor alpha2delta-1 is a neuronal thrombospondin receptor responsible for excitatory CNS synaptogenesis. *Cell* **139**, 380–392 (2009).
22. Fernandez, C., Tatard, V.M., Bertrand, N. & Dahmane, N. Differential modulation of Sonic-hedgehog–induced cerebellar granule cell precursor proliferation by the IGF signaling network. *Dev. Neurosci.* **32**, 59–70 (2010).
23. Heintzman, N.D. *et al.* Distinct and predictive chromatin signatures of transcriptional promoters and enhancers in the human genome. *Nat. Genet.* **39**, 311–318 (2007).
24. Wang, Z. *et al.* Combinatorial patterns of histone acetylations and methylations in the human genome. *Nat. Genet.* **40**, 897–903 (2008).
25. Mouse ENCODE Consortium. *et al.* An encyclopedia of mouse DNA elements (Mouse ENCODE). *Genome Biol.* **13**, 418 (2012).
26. Bao, D. *et al.* Cbln1 is essential for interaction-dependent secretion of Cbln3. *Mol. Cell. Biol.* **26**, 9327–9337 (2006).

27. Hirai, H. *et al.* Cbln1 is essential for synaptic integrity and plasticity in the cerebellum. *Nat. Neurosci.* **8**, 1534–1541 (2005).
28. Suzuki, K., Sato, M., Morishima, Y. & Nakanishi, S. Neuronal depolarization controls brain-derived neurotrophic factor-induced upregulation of NR2C NMDA receptor via calcineurin signaling. *J. Neurosci.* **25**, 9535–9543 (2005).
29. Perez-Pinera, P. *et al.* RNA-guided gene activation by CRISPR-Cas9-based transcription factors. *Nat. Methods* **10**, 973–976 (2013).
30. Visel, A., Minovitsky, S., Dubchak, I. & Pennacchio, L.A. VISTA Enhancer Browser: a database of tissue-specific human enhancers. *Nucleic Acids Res.* **35**, D88–D92 (2007).
31. Hambardzumyan, D. *et al.* AUF1 and Hu proteins in the developing rat brain: implication in the proliferation and differentiation of neural progenitors. *J. Neurosci. Res.* **87**, 1296–1309 (2009).
32. Vodopiutz, J. *et al.* Homozygous SALL1 mutation causes a novel multiple congenital anomaly-mental retardation syndrome. *J. Pediatr.* **162**, 612–617 (2013).
33. Warming, S., Rachel, R.A., Jenkins, N.A. & Copeland, N.G. Zfp423 is required for normal cerebellar development. *Mol. Cell. Biol.* **26**, 6913–6922 (2006).
34. Stergachis, A.B. *et al.* Developmental fate and cellular maturity encoded in human regulatory DNA landscapes. *Cell* **154**, 888–903 (2013).
35. Sheffield, N.C. *et al.* Patterns of regulatory activity across diverse human cell types predict tissue identity, transcription factor binding, and long-range interactions. *Genome Res.* **23**, 777–788 (2013).
36. Shalizi, A. *et al.* A calcium-regulated MEF2 sumoylation switch controls postsynaptic differentiation. *Science* **311**, 1012–1017 (2006).
37. Grinberg, I. *et al.* Heterozygous deletion of the linked genes ZIC1 and ZIC4 is involved in Dandy-Walker malformation. *Nat. Genet.* **36**, 1053–1055 (2004).
38. Aruga, J. The role of Zic genes in neural development. *Mol. Cell. Neurosci.* **26**, 205–221 (2004).
39. Borghesani, P.R. *et al.* BDNF stimulates migration of cerebellar granule cells. *Development* **129**, 1435–1442 (2002).
40. Kim, T.-H. *et al.* Broadly permissive intestinal chromatin underlies lateral inhibition and cell plasticity. *Nature* **506**, 511–515 (2014).
41. Samstein, R.M. *et al.* Foxp3 exploits a pre-existent enhancer landscape for regulatory T cell lineage specification. *Cell* **151**, 153–166 (2012).
42. Sotelo, C. Cellular and genetic regulation of the development of the cerebellar system. *Prog. Neurobiol.* **72**, 295–339 (2004).
43. Aruga, J., Inoue, T., Hoshino, J. & Mikoshiba, K. Zic2 controls cerebellar development in cooperation with Zic1. *J. Neurosci.* **22**, 218–225 (2002).
44. Aruga, J. *et al.* Mouse Zic1 is involved in cerebellar development. *J. Neurosci.* **18**, 284–293 (1998).
45. Zaret, K.S. & Carroll, J.S. Pioneer transcription factors: establishing competence for gene expression. *Genes Dev.* **25**, 2227–2241 (2011).
46. Ben-Arie, N. *et al.* Math1 is essential for genesis of cerebellar granule neurons. *Nature* **390**, 169–172 (1997).
47. Flora, A., Klisch, T.J., Schuster, G. & Zoghbi, H.Y. Deletion of Atoh1 disrupts Sonic Hedgehog signaling in the developing cerebellum and prevents medulloblastoma. *Science* **326**, 1424–1427 (2009).
48. John, S. *et al.* Chromatin accessibility pre-determines glucocorticoid receptor binding patterns. *Nat. Genet.* **43**, 264–268 (2011).
49. Camp, J.G. *et al.* Microbiota modulate transcription in the intestinal epithelium without remodeling the accessible chromatin landscape. *Genome Res.* **24**, 1504–1516 (2014).

ONLINE METHODS

Cerebellar immunostaining. C57BL/6Ncrl male or female mice (Charles River Labs) at P7, P14 or P60 were deeply anesthetized with isofluorane and their brains were dissected and flash frozen in OCT. Fresh frozen brains were cryostat sectioned in the sagittal plane at 18 µm, then fixed on slides in 4% paraformaldehyde (wt/vol) and rinsed with 1× phosphate-buffer saline (PBS). Slides were blocked in either 14% normal goat serum (vol/vol) or 10% normal donkey serum (vol/vol) (for primary antibodies raised in goat) and permeabilized in 0.3% Triton X-100 (vol/vol) before antibody incubation. Hoechst dye was used to label nuclei for identification of anatomical landmarks. Images were captured on a Leica DMI4000 inverted fluorescence microscope at 10× or 20× magnification with a Leica DFC-365 camera using Metamorph 7.0 software (Molecular Devices). We used the following primary antibodies: mouse anti-Ki67 (1:50; BD Pharmingen 550609), goat anti-Dcx (1:100, Santa Cruz sc-8066), rabbit anti-$GABA_AR\alpha6$ (1:1,000, Millipore AB5610), rabbit anti-Zic1/2 (1:1,000, R. Segal, Harvard Medical School[39]), mouse anti-GFAP (1:100, Abcam cat. #ab10062) and rabbit anti-calbindin (1:1,000, Swant cat. #CB38). Secondary antibodies were used at 1:500: donkey anti-goat Cy3 (Jackson ImmunoResearch, 705-165-003), goat anti-rabbit Cy2 (115-225-146), goat anti-mouse Cy3 (115-165-146) and goat anti-mouse Cy5 (115-175-146). All animals were housed in groups of 4–5, given access to standard laboratory chow and water *ad libitum* and housed in a humidity and temperature-controlled room on a 14/10-h light/dark cycle. All experiments were conducted in accordance with an approved protocol from the Duke University Institutional Animal Care and Use Committee and guidelines from the National Institutes of Health for the Care and Use of Laboratory Animals.

Isolation of cerebellar nuclei. For *in vivo* samples, C57BL/6Ncrl male and female mice at P7, P14 or P60 were deeply anesthetized with isofluorane and decapitated for brain harvesting. The cerebellar cortex was dissected, flash frozen, and stored at −80 °C. For CGN cultures (described below), neurons were scraped into PBS and harvested by centrifugation at 1,000*g* for 5 min. Nuclei were extracted essentially as previously described[50]. Briefly, each cerebellum was dounced in 5 ml 2 M sucrose, 1 mM $MgCl_2$ and poured through a 100-µm filter. Filtered tissue was ultracentrifuged in 15 ml of 2 M sucrose, 1 mM $MgCl_2$ at 65,000*g* for 80 min. Supernatant was removed and the tight nuclear pellet was resuspended by pipetting in 1 ml buffer RSB from the DNase-seq protocol[51]. Nuclei were quantified by hemocytometer, yielding approximately 5–10 million per adult cerebellum (~30 mg tissue).

DNase-seq library generation. DNase-seq libraries were constructed from nuclear preparations as previously described[51]. Briefly, 15–30 million nuclei were digested with a range of recombinant DNase I enzyme (Roche) concentrations (between 1.2 and 12 U) for 15 min at 37 °C in 120 µl 1× DNase buffer. Digestions were checked by pulse field gel electrophoresis and material was pooled from three different DNase concentrations (extent of digestion matched between samples) in equimolar amounts following blunt-ending reactions. Following ligation to adapters, MmeI digestion, streptavidin bead-based enrichment, and 14 cycles of PCR amplification, each library was sequenced for either 36 cycles on an Illumina GAIIx machine, or 50 cycles on a Hi-Seq 2000 platform to an average depth of 115 million aligned reads per sample. Nuclei from cerebellae of 4–6 mice or ~20 million cultured CGNs were pooled for each biological replicate, and three independent biological replicates were analyzed for each time point.

RNA isolation and sequencing. RNA was isolated from P7, P14 or P60 C57BL/6 mouse cerebellar cortex or cultured mouse CGNs using the Absolutely RNA kit (Agilent). For *in vivo* samples, RNA from at least two cerebellae was pooled for each biological replicate, and in culture a single litter constituted a biological replicate of cultured CGNs. Three independent biological replicates were analyzed for each time point. 2 µg of total RNA was used for standard TruSeq library preparation with polyA selection (performed by the Duke Sequencing and Analysis Core Resource). Libraries were subjected to 50 bp paired-end Illumina Hi-Seq 2000 sequencing, with the exception of Zic knockdown experiments, in which biological duplicates were sequenced as single-end 50 bp.

Cerebellar granule neuron culture. Granule neuron precursors were isolated and cultured as previously described[52]. Briefly, cerebellae from a litter of P7 mice were chopped into small pieces then digested at 37 °C for 30 min in 10 U ml^{-1} papain (Worthington), 200 g ml^{-1} L-cysteine (Sigma), and 250 U ml^{-1} DNase (Sigma) in PBS. The tissue was mechanically triturated in PBS with trypsin inhibitor and 250 U/ml DNase then centrifuged and resuspended in PBS/BSA. The cell suspension was passed through a cell strainer (Becton Dickinson), layered on a step gradient of 35% and 65% Percoll (Sigma), and centrifuged at 2,500 rpm for 12 min at 25 °C. Granule Neuron Precursors (GNPs) were harvested from the 35/65% interface, washed in PBS/BSA, resuspended in Neurobasal medium with B27 supplements and 2% FBS and plated on poly-D-lysine–coated dishes. In some cases as noted in the text, Brain-Derived Neurotrophic Factor (Peprotech) was added at 50 ng ml^{-1} on +4 DIV.

CGN immunostaining. For immunostaining, freshly isolated GNPs were plated on glass coverslips coated with poly-D-lysine and laminin in Neurobasal media with B27 supplements and 2% serum as above. Cells were then either fixed in 4% paraformaldehyde immediately (+0 DIV; GNPs) or allowed to differentiate for 3 or 7 DIV. Cells were blocked in 10% goat serum and permeabilized with 0.3% Triton X-100 before primary antibody application overnight. We used the following primary antibodies: mouse anti-Ki67 (1:50, BD Pharmingen 550609), chicken anti-MAP2 (1:200, Millipore AB5543), and rabbit anti-synaptophysin (1:500, Millipore MAB5258). Secondary antibodies labeled with Cy2, Cy3, or Cy5 were used at 1:500 (see "Cerebellar immunostaining"). Hoechst dye was used to label nuclei for cellular identification. Images were captured on a Leica DMI4000 inverted fluorescence microscope at 20× or 40× magnification with a Leica DFC-365 camera using Metamorph 7.0 software.

Luciferase reporter assays. Putative enhancers were cloned in the vector pGL3 (Promega). For *Cbln3,* we cloned mm9 region chr14:56500910–56501851, at the BglII site upstream of luciferase. For the two regions in the *Grin2c* interval on Chr. 11, we cloned the following mm9 regions at the BamHI or SalI sites downstream of the *luc*+ coding sequence: Site #1: chr11:115064061–115064510; Site #2: chr11:115128431–115128780. Luciferase reporters were transfected into cultured CGNs on +1 DIV by calcium phosphate precipitation as described[53]. Co-transfection of TK-renilla luciferase (Promega) was used to control for transfection efficiency and sample handling. As described in the text, in some cases plasmids encoding shRNAs targeting Zic1 in the vector *pLKO.1* or empty *pLKO.1* were co-transfected with the luciferase plasmids. Data presented are the average of at least three measurements from each of at least two independent experiments.

Chromatin immunoprecipitation. For ChIP we pooled cerebellum or cortex from three P7 mice or two P60 mice for each biological replicate. Brain samples were dounced in 1% formaldehyde (wt/vol) PBS buffer and kept at 25 °C for 15 min, washed twice with cold PBS, then lysed in 600 µl lysis buffer (1% SDS (wt/vol), 10 mM EDTA, and 50 mM Tris, pH 8.1). The crosslinked material was sonicated with a Bioruptor (Diagenode) with 30 s on/off cycles to an average size range of 150–350 bp as visualized by agarose gel electrophoresis. Sonicated supernatants were diluted tenfold in dilution buffer (0.01% SDS, 1.1% Triton X-100, 1.2 mM EDTA, 16.7 mM Tris-HCl, pH 8.1, 167 mM NaCl) before immunoprecipitation. 6 µl of antibody (anti-Zic 1/2 C terminus, courtesy of R. Segal, Harvard Medical School[39], total rabbit IgG, Millipore 12-370, or anti histone H3K27Ac, Abcam Ab472) was first incubated with 100 µl of Dynabeads Protein G (Invitrogen 10004D) beads for 4 h at 4 °C, then the antibody conjugate was added to 6 ml of cell lysis for overnight IP. Standard TruSeq adapters were ligated for library preparation, which for Zic used the MicroPlex Library Preparation Kit (Diagenode), and for H3K27ac used the NEB Library Preparation Kit (NEB 6240S and NEB E7335s). 50 bp single-end sequencing was performed at the Duke Sequencing and Analysis Core Resource on a Hi-Seq 2000 machine. Two independent biological replicates were performed for each antibody, developmental time point, and brain region.

RNA interference. For the knockdown of Zic1 and Zic2 transcription factors, we purchased shRNAs targeting mouse *Zic1* and *Zic2* that were cloned in the lentiviral vector *pLKO.1* (Thermo Scientific). *Zic1* shRNA (TRCN0000096685), *Zic2* shRNA (TRCN0000095251). Empty *pLKO.1* was used as the control. Viral shRNAs were packaged as lentivirus in HEK293T cells (ATCC) following standard procedures. Neurons were infected with lentivirus at a multiplicity of infection of 1 on +1 DIV, and samples were harvested for RNA or protein analysis on +7 DIV.

Quantitative RT-PCR. 800ng of total RNA was used for reverse transcription with oligo dT primers and Superscript II (Invitrogen). Quantitative SYBR green PCR was performed on an ABI 7300 real-time PCR machine (Applied Biosystems) using the following intron-spanning primers (IDT): *Grin2b*, F: GAGCATAATCACCCGCATCT, R: AAGGCACCGTGT- CCGTATCC; *Zic1,* F: CAGCCCGCGATCCGAGCACTATG, R: GCAGCCCTCG- AACTCG CACTTGAA; *Zic2,* F: GGCGGCGCAGCTCCACAACCAGTA, R: TTGCC ACAGCCCGGGAAAGGACAG; *Grin2c,* F: TGTGGGCCTTCTTCGCTGT-CATCT, R: TGCCATTAGGTACCGTGCCAAAAC; *Tubb5,* F: GGGAGG TGATAAG-CGATGAA, R: CCCAGGTTCTAGATCCACCA; *Gapdh,* F: CATGGCCTTCCGTGT-TCCT, R: TGATGTCATCATACTTGGCAGGTT. Each sample was measured in triplicate, and all data were normalized to the expression of the housekeeping gene *Gapdh*.

Western blotting. 1 million CGNs or 10 mg cerebellar or non-cerebellar brain tissue was lysed in RIPA buffer to a final concentration of 10 mg ml^{-1}, then disrupted by sonication. 100 µg total lysate was run for SDS-PAGE and transferred to nitrocellulose for western blotting. Actin was used as a loading control. Primary antibodies were mouse anti-Zic1/2 C terminus[39], mouse anti-Actin (1:10,000; Millipore MAB1501). Secondary antibodies were goat anti-rabbit 770 (Biotium 20078) and goat anti-mouse 680 (Biotium 20065). Bands were visualized with fluorescent secondary antibodies using the Odyssey imaging system (LI-COR Bioscience).

Cas9-based RNA-guided gene activation. The CRISPR web interface from the Zhang lab at MIT (http://crispr.mit.edu) was used to design CRISPR guide RNA (gRNA) followed by a PAM site (NGG) that have minimal off-target matches. We selected three gRNA sequences for each element tested (site #1: chr11:115064061–115064510; site #2: chr11:115128431–115128780). Oligonucleotides containing target sequences were obtained from IDTand cloned at the BsmBI site in a FUGW-based U6 chimeric gRNA expression vector co-expressing GFP. Site 1-1: GCTCCACACCTGCGGAGGTA, Site 1-2: GCACGCAAACCTCTACTGGGC, Site 1-3: GTTAGAAAGAAGGGCGTACGG, Site 2-1: GCACAGCCC CGCCGCGGGGCG, Site 2-2: GAGGGGCCAGCTAGGAGCAC, Site 2-3: GAGATGGAGCTCGCCACCGC. We used an enzymatically dead Cas9-VP64 fusion protein cloned in a lentiviral backbone with T2A expression of GFP (*pLV hUbC-dCas9VP64-T2A-GFP*; Addgene plasmid #53192). Constructs were packaged as lentivirus in HEK293T cells and CGNs were infected on +1 DIV with either dCas9-VP64 alone, a pooled set of the three gRNA viruses targeting one of the elements, or dCas9-VP64 together with one of the gRNA pools. RNA was harvested on +7 DIV for cDNA synthesis and quantitative PCR. For each treatment we analyzed at least three samples from at least two independent experiments. In addition to *Grin2c* and *Gapdh* primers above, we used the following primers: *Rab37*, F: ACTGGCATGAACGTGGAGTT, R: TAGGGGGTCACACAAAGGAG; *Tmem104,* F: AAGTAACCTCTTGGGCCAGC, R: CACCAGCCCGACATAA GGAG; *Fdxr,* F: CATTTACACAGACAGCCCGC, R: CTGCTCCATAAC TCAGCACCA.

DNase-seq alignments, peak calling and differential signal tests. DNase-seq reads were trimmed to the first 20 bp (fixed insert length generated by MmeI digest following first linker ligation in library preparation) and aligned to the NCBI37/mm9 reference genome using BWA[54], allowing a single mismatch and mapping up to four locations. Alignments were filtered for PCR artifacts and normalized, smoothened coverage tracks and discrete peak calls were generated by F-seq[55]. DHS sites were annotated to genic features using the mm9 UCSC Genes knownGene table. The R package DESeq v1.8.3 was used for signal normalization and calling differential DHS sites (exact test on negative binomial distributions) between conditions to take into account signal-to-noise ratios and variance between replicates across sequencing depth[56]. Raw read counts (defined by the first 5-prime base of each read) summed in the 250-bp windowed union of top 100,000 DHS peaks identified in the samples under consideration served as input to DESeq analysis. 250-bp windows with 50-bp overlaps were chosen for increased resolution within peak calls.

RNA-seq alignments and differential expression tests. Following quality score-based trimming and adaptor filtering, reads were aligned to the UCSC Genes mm9 reference transcriptome and then NCBI37/mm9 reference genome using Tophat with options –x 4 and –n 2 (ref. 57). All transcriptome assemblies produced by the alignments were combined with Cuffmerge before differential testing. Cuffdiff[58] was used for pairwise tests of differential expression between normalized gene read counts of Fragments Per Kilobase of exon per Million fragments mapped (FPKM) with the default significance threshold of FDR < 0.05 used for all analyses, except for comparisons with Zic knockdown experiments, which used FDR < 0.10. Normalized UCSC browser coverage was generated by conversion of bam format alignments to bp resolution bigWig files and scaling by total number of mapped reads.

RNA-seq expression pattern clustering. RNA-seq data was analyzed in part with the cummeRbund R package (http://compbio.mit.edu/cummeRbund/) operating on Cuffdiff ouputs. For cluster profiles, all significantly differential genes from the *in vivo* time course were clustered by JS distance to a priori defined expression vectors (for example, [0, 1, 0] for elevated expression in P14 relative to P7 and P60). The 100 best match genes from each vector were plotted and subjected to the Database for Annotation, Visualization and Integrated Discovery (DAVID) to find enriched Cellular Component and Biological Process gene ontologies[59]. Principal components analyses (PCA) of gene expression were performed in cummeRbund.

Relationship between differential DHS and gene expression changes. To link differential DHS sites with gene expression changes, each DHS site was associated with its nearest UCSC mm9 reference gene. The fold change in each gene's FPKM values from P7 to P60 for *in vivo*, or GNPs to +7 DIV for cultured neurons were calculated. The distribution of fold changes was plotted as a cumulative function and two-sided Mann-Whitney tests between distributions assessed significance. DHS sites mapping within 2 kb of an annotated TSS were considered promoter-located and all other DHS sites were considered distal.

ENCODE histone mark ChIP-seq data sets. H3K27ac, H3K4me1 and H3K4me3 ChIP-seq data from P56 C57BL/6 cerebellum were retrieved from the Mouse ENCODE project August 2012 release from Ludwig Institute for Cancer Research (B. Ren laboratory). Available peak call files were used for determining overlap fractions with DHS sites in this study.

Cell type–enriched gene expression comparisons. Purkinje cell, Bergmann glia, and granule neuron (CGN) enriched gene lists were obtained from[14]. Sequenced RNA abundances captured with translating polysomes (TRAP-seq) in each cell type were compared with the DESeq package. This included 922 Purkinje cell, 2084 Bergmann glia, and 986 CGN enriched genes. For beanplots of DNase-seq, H3K27ac, and H3K4me3 signal, total read counts were extracted for each gene within 2 kb of the TSSand normalized by total aligned reads in that sample. Replicates were summed. Genes with FPKM between 0 and 1 were considered "low" expression, and FPKM > 1 considered "high." Significance assessed with two-sided Mann-Whitney test. To associate cell type enriched genes with differential DHS sites, differential DHS sites between P7 and P60 cerebellum were each assigned a single nearest gene and the percent overlap of this list with cell type enriched genes that also displayed differential expression between P7 and P60 was computed. These percentages were compared to the percent overlap obtained from random sampling from all expressed genes (10,000 iterations).

Motif-finding in DHS sites. Enriched motifs in differential DHS sites were identified using MEME-ChIP[60] with a third-order Markov model background of all DHS sites. The top 10 Discriminative DNA Motif Discovery (DREME) hits by e-value were selected and aligned to known motifs contained in the JASPAR vertebrates and UniPROBE mouse databases.

Vista Enhancer Browser analyses. The VISTA Enhancer Browser was accessed October 10, 2013 while containing 1,940 total tested putative enhancer elements[30]. The top 75,192 DHS sites from P7 cerebellum, adult mouse heart, liver, and kidney DNase-seq were overlapped with all VISTA tested elements that showed reproducible staining in hindbrain or heart. All VISTA tested elements overlapping P7 DHS sites are provided in **Supplementary Table 8**. When associating VISTA elements with genes, we used the nearest reference gene and ignored any gene annotation that showed zero expression by RNA-seq across time points.

H3K27ac and Zic ChIP-seq analysis. 50-bp SR ChIP-seq reads were aligned to the NCBI37/mm9 reference genome with Bowtie, allowing up to two mismatches

doi:10.1038/nn.3995

and requiring unique alignments. bigWig coverage tracks were normalized by total number of mapped reads. Captured fragment length shifts were estimated for each library by cross-strand correlation maxima[61,62] and used for peak calling with MACS v1.4.2 (ref. 63) with matched input controls and default $P < 0.00001$ threshold for each replicate. Cross-strand correlation maxima were also used for quality control to assess signal to noise ratio of each ChIP-seq experiment and samples displaying low scores were omitted. For differential Zic binding detection, raw read counts mapped to the union of Zic ChIP-seq peak calls for all P7 and P60 replicates were used as input to DESeq[56]. Differential binding events between P7 and P60 were determined by DESeq negative binomial test at a FDR < 0.05 threshold. To correlate with expression changes observed, Zic binding sites were linked to the nearest expressed gene.

Statistical analysis. Individual statistical tests employed are noted in figure legends. Two-sided unpaired *t* tests were used for comparisons of normal distributions and Mann-Whitney or exact tests were used for non-normally distributed sequencing data. No statistical methods were used to predetermine sample sizes but our sample sizes are similar to those reported in previous studies[14,49,64]. Data collection and analysis were not performed blind to the conditions of the experiments. Order of sequencing sample collection was random but no other randomization of data was performed.

A **Supplementary Methods Checklist** is available.

50. Thomas, J.O. & Thompson, R.J. Variation in chromatin structure in two cell types from the same tissue: a short DNA repeat length in cerebral cortex neurons. *Cell* **10**, 633–640 (1977).
51. Song, L. & Crawford, G.E. DNase-seq: a high-resolution technique for mapping active gene regulatory elements across the genome from mammalian cells. *Cold Spring Harb. Protoc.* **2010**, pdb.prot5384 (2010).
52. Kokubo, M. *et al.* BDNF-mediated cerebellar granule cell development is impaired in mice null for CaMKK2 or CaMKIV. *J. Neurosci.* **29**, 8901–8913 (2009).
53. Tao, X., West, A.E., Chen, W.G., Corfas, G. & Greenberg, M.E. A calcium-responsive transcription factor, CaRF, that regulates neuronal activity-dependent expression of BDNF. *Neuron* **33**, 383–395 (2002).
54. Li, H. & Durbin, R. Fast and accurate short read alignment with Burrows-Wheeler transform. *Bioinformatics* **25**, 1754–1760 (2009).
55. Boyle, A.P., Guinney, J., Crawford, G.E. & Furey, T.S. F-Seq: a feature density estimator for high-throughput sequence tags. *Bioinformatics* **24**, 2537–2538 (2008).
56. Anders, S. & Huber, W. Differential expression analysis for sequence count data. *Genome Biol.* **11**, R106 (2010).
57. Trapnell, C., Pachter, L. & Salzberg, S.L. TopHat: discovering splice junctions with RNA-Seq. *Bioinformatics* **25**, 1105–1111 (2009).
58. Trapnell, C. *et al.* Transcript assembly and quantification by RNA-Seq reveals unannotated transcripts and isoform switching during cell differentiation. *Nat. Biotechnol.* **28**, 511–515 (2010).
59. Huang, D.W., Sherman, B.T. & Lempicki, R.A. Systematic and integrative analysis of large gene lists using DAVID bioinformatics resources. *Nat. Protoc.* **4**, 44–57 (2009).
60. Machanick, P. & Bailey, T.L. MEME-ChIP: motif analysis of large DNA datasets. *Bioinformatics* **27**, 1696–1697 (2011).
61. Kharchenko, P.V., Tolstorukov, M.Y. & Park, P.J. Design and analysis of ChIP-seq experiments for DNA-binding proteins. *Nat. Biotechnol.* **26**, 1351–1359 (2008).
62. Landt, S.G. *et al.* ChIP-seq guidelines and practices of the ENCODE and modENCODE consortia. *Genome Res.* **22**, 1813–1831 (2012).
63. Zhang, Y. *et al.* Model-based analysis of ChIP-Seq (MACS). *Genome Biol.* **9**, R137 (2008).
64. Paige, S.L. *et al.* A temporal chromatin signature in human embryonic stem cells identifies regulators of cardiac development. *Cell* **151**, 221–232 (2012).